Regulation of the expression of the nickel uptake system in *Vibrio cholerae* by iron and heme via Fur

Kazuyoshi Muranishi [a], Koichiro Ishimori [a,b], and Takeshi Uchida [a,b,*]

[a] *Graduate School of Chemical Sciences and Engineering, Hokkaido University, Sapporo 060-8628, Japan*

[b] *Department of Chemistry, Faculty of Science, Hokkaido University, Sapporo 060-0810, Japan*

[*]Corresponding author

E-mail address: uchida@sci.hokudai.ac.jp (T. Uchida)

ABSTRACT

Fur (ferric uptake regulator) is a transcription factor that regulates expression of downstream genes containing a specific Fe^{2+}-binding sequence called the Fur box. In *Vibrio cholerae*, a Fur box is located upstream of the *nik* operon, which is responsible for nickel uptake, suggesting that its expression is regulated by Fur. However, there are no reports that Ni^{2+} induces expression of Fur box genes. Accordingly, we here investigated whether Ni^{2+} or Fe^{2+} binds to Fur to regulate expression of the *nik* operon. We found that Fur binds to the Fur box in the presence of Fe^{2+} with a dissociation constant (K_d) of 1.2 μM, whereas only non-specific binding was observed in the presence of Ni^{2+}. Thus, Fur-mediated expression of the *nik* operon is dependent on Fe^{2+}, but not Ni^{2+}. Since most iron in cells exists as heme, we examined the effect of heme on the Fur box binding activity of *V. cholerae* Fur (*Vc*Fur). Addition of heme to the *Vc*Fur-Fur box complex induced dissociation of *Vc*Fur from the Fur box, indicating that expression of the *V. cholerae nik* operon is regulated by both iron and heme. Furthermore, VCA1098, a *nik* operon-encoded protein, bound heme with a K_d of 1.3 μM. Collectively, our results suggest that the *V. cholerae nik* operon is involved not only in nickel uptake but also in heme uptake, and depends on iron and heme concentrations within bacteria.

Keywords: Ferric uptake regulator, *Vibrio cholerae*, *nik* operon

1. Introduction

The nickel-uptake system plays a crucial role in the survival of some bacteria; one well-known example is the human gastric pathogen *Helicobacter pylori* [1]. *H. pylori* utilizes urease, a nickel-containing protein, to produce ammonia, which neutralizes the local strong acid environment in the stomach; thus, it requires efficient acquisition of nickel from the environment [2–6]. A nickel-uptake system has also been found in other bacteria, including the well-studied *Escherichia coli*. The nickel uptake system of *E. coli* consists of five proteins encoded by the *nik* operon (NikA-E) (Fig. 1) [7]. NikA is a periplasmic binding protein that chelates free nickel via a nickelophore [8]; NikB and NikC are periplasmic permeases; and NikD and NikE are ATPase subunits. Transcription of the *nik* operon is controlled by nickel-response regulator (NikR) in response to intracellular nickel concentration [9] and is enhanced under anaerobic conditions through fumarate and nitrate regulatory protein (FNR) [10].

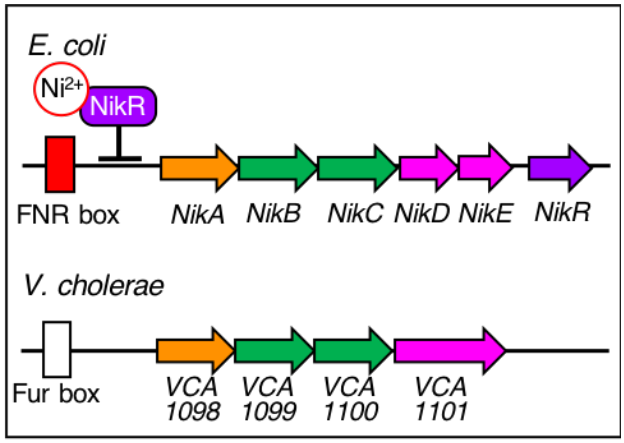

Fig. 1. Comparison of the *nik* operon between *E. coli* K-12 and *V. cholerae* O1 El Tor. Genes and arrows indicating the extent of the *nik* operons are color-coded to facilitate comparison. Proteins localized in the periplasm are displayed in orange, transmembrane proteins are displayed in green, and proteins localized in the cytoplasm are displayed in magenta. The *nikR* gene, located downstream of the FNR box in *E. coli* but absent in *V. cholerae*, is colored purple. A Fur box (white box) is located upstream of the *nik* operon of *V. cholerae*, whereas a FNR box (red box) is located upstream of the *nik* operon of *E. coli*. Filled arrows are drawn to scale and accurately positioned based on the genome sequences depicted.

Orthologs of *nik* operon genes are present in *Vibrio cholerae*. These genes encode VCA1098, VCA1099, VCA1100 and VCA1101, which correspond to NikA, NikB, NikC and NikDE of *E. coli*, respectively (Fig. 1). However, because the *nik* operon in *V. cholerae* lacks an upstream FNR-binding motif, the mechanism that regulates the nickel-uptake system in *V. cholerae* is clearly different from that in *E. col*. Furthermore, the gene corresponding to *nikR* in *E. coli* is not present in *V. cholerae*. Instead, a ferric-uptake regulator (Fur) protein binding motif exists 10 base pairs upstream of VCA1098. A previous study reported that a Fur mutation increases the expression of VCA1098 by 2.6-fold [11], suggesting that Fur regulates the expression of the *nik* operon in *V. cholerae*. However, there are no reports that the *nik* operon is involved in iron uptake, and the reason why a Fur-binding motif is present upstream of the *nik* operon is not clear. Fur acts as an intracellular iron level-dependent transcriptional regulator of numerous genes [12]. Fur has also been shown to bind to a DNA sequence known as the Fur box, even in the presence of divalent metals such as Zn^{2+}, Mn^{2+} and Fe^{2+} [13]. Therefore, it is possible that Fur senses nickel in *V. cholerae* and regulates the expression of the *nik* operon.

In this work, we investigated whether Ni^{2+} or Fe^{2+} regulates expression of the *nik* operon in *V. cholerae* via Fur. The binding affinity of Fur for the Fur-binding motif in the presence of Ni^{2+}, Fe^{2+} or Mn^{2+} was evaluated by fluorescence anisotropy. These studies revealed that Ni^{2+} does not specifically promote Fur recognition of the Fur box, whereas Fe^{2+} does. This metal selectivity reflects difference in tertiary structure: Fe^{2+} maintains binding of the Fur dimer to DNA, whereas Ni^{2+} maintains binding of the Fur tetramer to DNA. Collectively, these data suggest that Fur regulates expression of nickel-uptake proteins in *V. cholerae* in response to the concentration of Fe^{2+}.

2. Material and methods

2.1 *Materials*

The chemicals used in this study were purchased from FUJIFILM Wako Pure Chemical Industries (Osaka, Japan), Nacalai Tesque (Kyoto, Japan) or Sigma-Aldrich (St. Louis, MO, USA), and used without further purification.

2.2 *Expression and purification of VcFur*

The *fur* gene from *V. cholerae*, with codons optimized for *E. coli* expression, was purchased from Eurofins Genomics (Tokyo, Japan) and amplified by polymerase chain reaction (PCR) and cloned into a pGEX-6P-1 vector (Cytiva, Uppsala, Sweden). The expression plasmid was transformed into the *E. coli* C43(DE3) strain (Lucigen, Middleton, WI) and cultured at 37 °C in Luria-Bertani (LB) broth supplemented with 100 μg mL^{-1} ampicillin. After optical density at 600 nm (OD_{600}) of the culture reached 0.8, expression of the glutathione-S-transferases (GST)-tagged protein was induced with 0.4 mM isopropyl β-D-thiogalactopyranoside (IPTG). The cells were further grown at 28 °C overnight, then harvested by centrifugation and stored at -80 °C until use. The pellet was subsequently thawed on ice; suspended in lysis buffer containing 50 mM Tris-HCl, 500 mM NaCl (pH 8.0), 0.1% Nonidet P-40, 1 mg mL^{-1} lysozyme and DNase; and incubated on ice for 60 min. The sample was centrifuged at 40,000 × g for 30 min, and the supernatant was mixed with 5.0 mL of COSMOGEL GST-accept agarose (Nacalai Tesque, Japan) and incubated for 1 h at 4 °C with gentle agitation. The slurry was poured onto a column and washed with 50 mL wash buffer (50 mM Tris-HCl and 150 mM NaCl, pH 8.0). The GST-tag was cleaved by re-suspending beads in 10 mL cleavage buffer (50 mM Tris-HCl, 150 mM NaCl, 1 mM EDTA and 1 mM dithiothreitol (DTT), pH 8.0) containing 10 μg human rhinovirus 3C (HRV3C) protease and incubating at 4 °C overnight. After cleavage, the slurry was poured onto a column and the flow-through was collected. Collected *Vc*Fur was concentrated to 2 mL using a Vivaspin Turbo (MWCO, 10,000; Sartorius, Göttingen Germany) and applied to a HiLoad 16/600 Superdex 200 gel-filtration column (Cytiva) pre-equilibrated with 50 mM Tris-HCl/150 mM NaCl (pH 8.0) using an ÄKTA pure (Cytiva) liquid

chromatography apparatus. Protein purity was assessed by sodium dodecyl sulfate-poly acrylamide gel electrophoresis (SDS-PAGE) on 15% polyacrylamide gels. Metal content was determined using inductively coupled plasma-atomic emission spectrometry (ICP-AES) (ICPE-9000; Shimadzu Co., Japan). To reconstitute *Vc*Fur with Fe^{2+} or Ni^{2+}, 100 μM $Fe(NH_4)_2(SO_4)_2$ or $NiCl_2$ was added to 50 μM purified *Vc*Fur and incubated for 5 min at 4 °C. The sample was treated with a PD-10 desalting column (Cytiva) to remove free metals, then ICP measurements were performed to determine the metal contents. For the reconstruction of Mn^{2+}, 1 mM $MnCl_2$ was added to 50 μM *Vc*Fur, incubated for 5 min at 4 °C, and dialyzed overnight.

2.3 *Fluorescence anisotropy spectroscopy*

An HPLC-grade 6-carboxyfluorescein (6-FAM)-labeled Fur box motif of the *V. cholerae nik* operon gene (5'-TAG ACA TGA TTT TTA TTC TCA TGC T-3', with complementary sequence), purchased from Eurofins Genomics, was used as the target DNA oligomer for fluorescence anisotropy measurements. This target DNA oligomer, designated 6-FAM–labeled Fur box, was dissolved in 10 mM Tris-HCl, 50 mM NaCl, and 1 mM EDTA (pH 7.5). The 6-FAM–labeled Fur box was annealed by first heating to 95 °C for 5 min and then cooling to 25 °C for ~2 h using a GeneAmp 9700 thermocycler (Applied Biosystems, USA). The 6-FAM–labeled Fur box thus prepared was stored at -20 °C until use.

Fluorescence anisotropy was measured at excitation and emission wavelengths of 495 nm and 517 nm, respectively, using a FP-8500 spectrofluorometer (JASCO, Japan). Slit width for excitation and emission were set to 5 and 10 nm, respectively. *Vc*Fur titrations with 6-FAM–labeled Fur box were conducted in binding buffer (40 mM HEPES, 40 mM KCl, 20% glycerol, 100 μg mL^{-1} bovine serum albumin [BSA] and 0–200 μg mL^{-1} sheared salmon sperm DNA at pH 7.5) at 20 °C using a 6-FAM–labeled Fur box concentration of 50 nM. Anisotropy was measured after the sample mixture had been incubated for 15 min at 37 °C and then cooled to

5 °C for 5 min. Total fluorescence anisotropy was calculated using equation 1,

$$Anisotropy\ (r) = \frac{I_{\mathrm{VV}} - GI_{\mathrm{VH}}}{I_{\mathrm{VV}} - 2GI_{\mathrm{VH}}}, \quad (1)$$

where *I* is fluorescence intensity and V and H denote vertical and horizontal, respectively. The first and second characters of the subscript are polarization direction of excitation and emission light, respectively; and *G* is an instrument correction factor determined by excitation of binding buffer containing 50 nM 6-FAM–labeled Fur box. Binding curves were analyzed with a ligand-binding equation (equation 2) or double-Hill equation (equation 3) using IGOR Pro (WaveMetrics, Lake Oswego, OR, USA).

$$r = r_{\mathrm{base}} + (r_{\mathrm{max}} - r_{\mathrm{base}}) \frac{[\mathrm{DNA}] + [\mathrm{Fur}] + K_{\mathrm{d}} - \sqrt{([\mathrm{DNA}] + [\mathrm{Fur}] + K_{\mathrm{d}})^2 - 4[\mathrm{DNA}][\mathrm{Fur}]}}{2[\mathrm{Fur}]} \quad (2)$$

$$Anisotropy = \mathrm{C} + \sum_{x=1}^{2} \left\{ \mathrm{base}_x + \frac{\mathrm{max}_x - \mathrm{base}_x}{1 + \left(\frac{K_{d,x}}{[Vc\mathrm{Fur}]} \right)^{n_x}} \right\} \quad (3)$$

2.4 *Spectroscopy*

Circular dichroism (CD) spectra were obtained at room temperature with a J-1500 CD spectrometer (JASCO) over a spectral range of 190–250 nm using a One-Drop microsampling disc (JASCO) with a path length of 0.2 mm. Samples were diluted to a final concentration of 100 μM in 10 mM Tris-HCl (pH 7.5).

2.5 *Size-exclusion chromatography*

Protein oligomerization was analyzed using an ENrich 650 gel-filtration column (Bio-Rad Laboratories, Inc. Hercules, CA), equilibrated with 40 mM HEPES, 40 mM KCl and 20% glycerol (pH 7.5), using an ÄKTA explorer 10S liquid chromatography apparatus. The elution profile was monitored at 260 and 280 nm. Samples were calibrated by applying standards with

known molecular masses (ferritin, 440,000 Da; catalase, 232,000 Da; ovalbumin, 158,000 Da; bovine serum albumin, 66,000 Da; ovalbumin, 43,000 Da; ribonuclease A, 13,700 Da; and blue dextran, 2,000 kDa) (Gel Filtration Calibration Kits, Cytiva) to the column.

2.6 *Heme titration*

Fluorescence spectra were obtained at 25 °C using a FP-8500 spectrofluorometer (JASCO). All spectra were recorded in a 3 mL quartz cuvette in 50 mM Tris-HCl/150 mM NaCl (pH 8.0). For *Vc*Fur, the excitation wavelength was 275 nm and emission spectra were recorded over the range of 280–450 nm; for VCA1098, the excitation wavelength was 290 nm and emission spectra were recorded over the range of 310–450 nm. Excitation and emission slits were set to 10 nm. Binding titration data were fitted to equation 4, which assumes a single binding site:

$$F_{\mathrm{obs}} = F_0 + (F_{\mathrm{max}} - F_0)\frac{[\mathrm{L}]_\mathrm{T} + [\mathrm{E}]_\mathrm{T} + K_\mathrm{d} - \sqrt{([\mathrm{L}]_\mathrm{T} + [\mathrm{E}]_\mathrm{T} + K_\mathrm{d})^2 - 4[\mathrm{L}]_\mathrm{T}[\mathrm{E}]_\mathrm{T}}}{2[\mathrm{E}]_\mathrm{T}} \quad (4)$$

where F_{obs} is the observed fluorescence; F_0 is the initial fluorescence; F_{max} is the maximum amplitude of fluorescence quenching; $[\mathrm{L}]_\mathrm{T}$ and $[\mathrm{E}]_\mathrm{T}$ are total ligand and protein concentrations, respectively; and K_d is the apparent dissociation constant of the protein for heme.

2.7 *Overexpression and purification of VCA1098*

The full-length *vca1098* gene, with codons optimized for *E. coli* expression, was purchased from Eurofins Genomics and cloned into a modified pET-28b vector (Merck Millipore) using *Nde*I and *Eco*RI restriction sites, in which the existing thrombin recognition site composed of Leu-Val-Pro-Arg-Gly-Ser was mutated to the HRV 3C protease recognition site, Leu-Glu-Val-Leu-Phe-Gln-Gly-Pro, as described previously [14]. *E. coli* strain BL21(DE3) (Nippon Gene, Tokyo, Japan) carrying an expression plasmid for *vca1098* was grown at 37 °C in LB medium supplemented with 50 μg mL^{-1} kanamycin. Expression of the His_6-tagged fusion protein in *E. coli* was induced with 0.8 mM IPTG after reaching an OD_{600} of 0.8, and cultures were further

grown at 28 °C overnight. The cells were harvested by centrifugation and stored at -80 °C until use. The pellet was subsequently thawed on ice, suspended in lysis buffer, and incubated on ice for 60 min. The sample was then centrifuged at 40,000 × g for 30 min, and the resulting supernatant was resolved on a HisTrap HP column (Cytiva), pre-equilibrated with 50 mM Tris-HCl buffer containing 500 mM NaCl (pH 8.0), using an ÄKTAprime plus (Cytiva) liquid chromatography apparatus. The resin was extensively washed with a buffer consisting of 50 mM Tris-HCl, 500 mM NaCl and 50 mM imidazole (pH 8.0), and bound protein was eluted in 50 mM Tris-HCl buffer containing 500 mM NaCl and 200 mM imidazole (pH 8.0). The His_6-tag in VCA1098 was cleaved by incubating eluted VCA1098 with HRV 3C protease at 4 °C for ~16 h. After cleavage, the reaction mixture was again applied to the HisTrap column. The column flow-through was collected and applied to a HiLoad 16/60 Superdex 200 gel-filtration column equilibrated with 50 mM Tris-HCl/150 mM NaCl (pH 8.0). Protein purity was assessed by SDS-PAGE on 12.5% polyacrylamide gels.

3. Results

3.1 *Cloning, expression, and purification of VcFur*

V. cholerae Fur (*Vc*Fur) was expressed in *E. coli* strain C43(DE3) and purified using GST affinity and size-exclusion chromatography. The protein used in this study was approximately ~95% pure based on SDS-PAGE analysis (Fig. 2A). The purified protein migrated as a single band with a molecular mass of 17 kDa, in good agreement with the calculated molecular mass of *Vc*Fur (16.9 kDa). Size-exclusion chromatography analyses showed that the molecular weight of the purified protein under native conditions was ~40 kDa, indicating that it is present as a dimer (Fig. 2B).

According to a previously reported crystal structure of *Vc*Fur protein [15], each monomer of dimeric *Vc*Fur contains two metal binding sites—a high-affinity site and a lower-affinity

site—occupied by zinc (Fig. S1). Of these two sites, the one with higher affinity is called the structural site, and the one with lower affinity is called the regulatory site (Fig. S1) [15]. Since the pattern of metal ion binding to Fur depends on culture and purification conditions, we determined the number of bound metal ions using inductively coupled plasma-atomic emission spectrometry (ICP-AES). This analysis revealed that purified *Vc*Fur contained 1.0 ± 0.1 mol of Zn per mol of *Vc*Fur monomer, which is henceforth referred to as Zn_1Fur. One additional metal ion can bind to Zn_1Fur. After reconstitution with Fe^{2+}, Mn^{2+} or Ni^{2+}, the ratios of the metals to Zn^{2+} were 1.8, 1.7 or 2.0, respectively. Although excess amounts of metals were bound to the protein, we did not purify them further because the reconstituted metals were easily dissociated from the protein after desalting or dialysis. Thus, we used these proteins as Zn_1M_1Fur (M is Fe^{2+}, Mn^{2+} or Ni^{2+}).

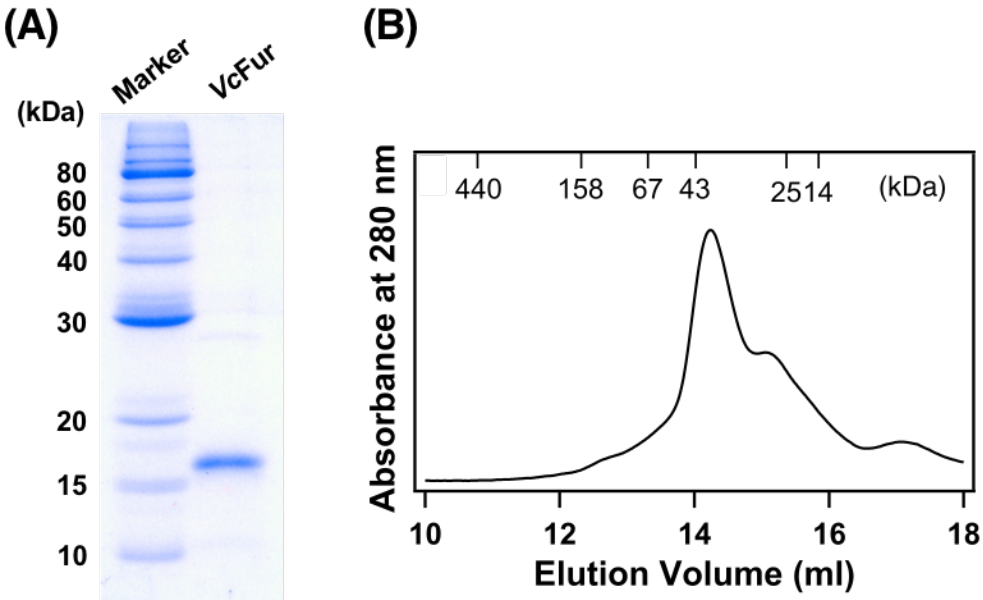

Fig. 2. (A) Representative Coomassie Brilliant Blue-stained SDS-PAGE gel showing purified *Vc*Fur. (B) Elution profile of purified *Vc*Fur on a Bio-Rad Enrich SEC 650 column monitored at 280 nm.

3.2 *Metal selectivity of Fur for Fur-box binding*

Because a Fur box sequence is present upstream of the *nik* operon, we investigated whether

Ni^{2+} activates *Vc*Fur by assessing DNA binding of *Vc*Fur based on the fluorescence anisotropy of 5'-6-FAM–labeled oligonucleotide. The anisotropy of the 6-FAM–labeled Fur box oligonucleotide was 0.07, which increased to 0.15 upon addition of Zn_1Fur up to a concentration of 60 μM (Fig. 3A, open circles).

Next, we measured the anisotropy of the 6-FAM–labeled Fur box in the presence of Ni^{2+}, which binds to the empty metal binding site of Zn_1Fur to form Zn_1Ni_1Fur. The fluorescence anisotropy of the 6-FAM–labeled Fur box increased from 0.10 to ~0.3 with increasing concentrations of Zn_1Ni_1Fur (Fig. 3A, filled circles). Fitting the anisotropy data to the ligand-binding equation (Eq. 2) failed because of divergence. Instead, the anisotropy data were fitted well to the sum of two Hill equations (Eq. 3), indicating biphasic binding with two different apparent dissociation constants (K_d). The calculated K_d values were 0.5 ± 0.1 and 1.3 ± 0.1 μM with the same Hill constant of 1.4 ± 0.1. Because the K_d value of *Ec*Fur is 0.020 μM, which is ~25-fold smaller than that of *Vc*Fur [13], it is possible that the value we obtained reflected non-specific binding. Thus, to confirm whether Zn_1Ni_1Fur binds specifically or non-specifically to the Fur box, we added sheared salmon sperm DNA (ssDNA) to the 6-FAM–labeled Fur box to suppress non-specific binding [16]. Plots were shifted to the right by the addition of ssDNA (Fig. 3A, filled triangles) compared with those obtained in the absence of ssDNA (Fig. 3A, filled circles) and were similar to those obtained in the absence of Ni^{2+} (Fig. 3A, open circles). At an ssDNA concentration of 200 μg mL^{-1}, the K_d value for the high-affinity site was increased by 10-fold (4.9 ± 0.1 μM), but the K_d for the low-affinity site could not be determined because the anisotropy was not saturated, even at 60 μM *Vc*Fur. These results show that binding of Zn_1Ni_1Fur to the Fur box was inhibited by ssDNA. Therefore, we attribute the increase in the anisotropy of Zn_1Ni_1Fur to non-specific binding of *Vc*Fur to the Fur box.

Since Fur is an iron-responsive regulator, we next measured anisotropy in the presence of 1 mM Fe^{2+} (Zn_1Fe_1Fur). To suppress the oxidation of ferrous iron, which interferes with the measurements by forming a precipitate, we added 10 mM ascorbic acid to the solution. The

anisotropy of the 6-FAM–labeled Fur box increased with increasing concentrations of Zn_1Fe_1Fur, exhibiting biphasic binding behavior with two different K_d values (Fig. 3B). Fitting the binding curves with the double-Hill equation (Eq. 3) yielded K_d values of 0.99 ± 0.1 and 18.1 ± 0.3 μM for high- and low-affinity sites, respectively, with corresponding Hill constants of 2.5 ± 0.1 and 2.7 ± 0.1. To suppress non-specific binding, we added ssDNA at a final concentration of 200 μg mL^{-1}. In the presence of ssDNA, anisotropy at Zn_1Fe_1Fur concentrations <6 μM largely overlapped that in the absence of ssDNA (Fig. 3B). In contrast, at concentrations of Zn_1Fe_1Fur >6 μM, anisotropy increased only slightly (from 0.15 to 0.18) as the concentration of Zn_1Fe_1Fur increased. To determine K_d values, we fitted the binding curve with the double-Hill equation (Eq. 3). The resulting K_d value of 1.2 ± 0.1 μM was comparable to that of the smaller K_d in the presence of ssDNA. In contrast, the K_d of the lower-affinity site could not be determined. Collectively, these results indicate that Zn_1Fe_1Fur binds specifically to DNA at concentrations less than 6 μM.

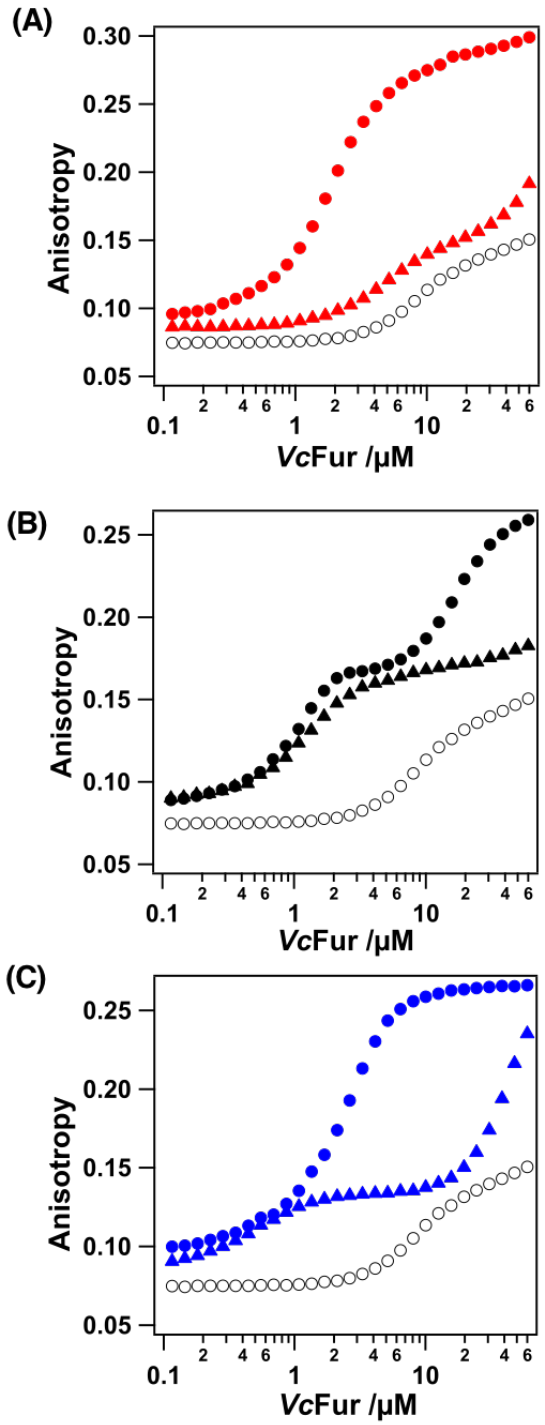

Fig. 3. Binding of *Vc*Fur to the Fur box. Fluorescence anisotropy data of (A) Zn_1Ni_1Fur, (B) Zn_1Fe_1Fur, and (C) Zn_1Mn_1Fur. Titration was performed using 50 nM 6-FAM–labeled Fur box. In each graph, the anisotropy of Zn_1Fur is shown by open circles. The anisotropy of metal-bound *Vc*Fur (Zn_1M_1Fur) in the absence and presence of 200 μg mL^{-1} of ssDNA is shown as filled circles and triangles, respectively.

We also examined binding behavior in the presence of Mn^{2+} (Zn_1Mn_1Fur). Anisotropy of the Fur box increased with increasing concentrations of Zn_1Mn_1Fur and showed biphasic

binding behavior with two different K_d (Fig. 3C). This behavior is similar to that of Zn_1Ni_1Fur (Fig. 3A), although non-specific binding of Zn_1Fe_1Fur was observed at concentrations greater than 10 μM. Application of the double-Hill equation to plots of anisotropy in the presence of ssDNA yielded a K_d value of 0.51 ± 0.01 μM, indicating that Zn_1Mn_1Fur also specifically binds to the Fur box at concentrations <10 μM. These results show that Fe^{2+} and Mn^{2+} activate *Vc*Fur but Ni^{2+} does not, suggesting that Ni^{2+} is not involved in regulating the expression of *nik* operon genes in *V. cholerae*. We examined binding of Zn_1Fe_1Fur, Zn_1Ni_1Fur and Zn_1Mn_1Fur to the Fur box using native-PAGE. Fig. S2 shows that Zn_1Fe_1Fur and Zn_1Mn_1Fur specifically bind to the Fur box, but a non-specific binding was increased in the case of Zn_1Ni_1Fur. The results obtained by native-PAGE are in close agreement with those obtained by fluorescence anisotropy (Fig. 3).

3.3 *Conformational changes in VcFur associated with metal binding*

To clarify the reason for metal-dependent DNA binding of *Vc*Fur, we examined structural changes induced by metal binding, first investigating secondary structural changes that occur upon metal binding. Measurements of far-UV circular dichroism (CD) spectra of *Vc*Fur showed that Zn_1Fur displayed minima at 208 and 227 nm and a maximum at ~196 nm, characteristic of a protein with a high α-helical content (Fig. 4A). The addition of 1 mM Fe^{2+} to Zn_1Fur did not alter the CD spectrum, indicating that Fe^{2+} induced almost no changes in the secondary structure of Zn_1Fur; Mn^{2+} similarly caused little change in the CD spectrum. In contrast, addition of 1 mM Ni^{2+} to Zn_1Fur increased the value of molar ellipticity at 208 and 227 nm by 44% and 25%, respectively, indicating loss of α-helical content upon Ni^{2+} binding.

Next, we examined the assembly state of *Vc*Fur by size-exclusion chromatography. Zn_1Fur eluted at 14.3 mL (Fig. 4B), which corresponds to a species with a molecular mass of ~40 kDa. Thus, Zn_1Fur exists as a dimer, as previously shown [15]. Addition of Fe^{2+} or Mn^{2+} to Zn_1Fur caused little change in the chromatogram (Fig. 4B), with Zn_1Fe_1Fur and Zn_1Mn_1Fur eluting at

14.2 and 14.1 mL, respectively, again corresponding to a molecular mass of ~40 kDa. Therefore, Zn_1Fe_1Fur and Zn_1Mn_1Fur also exist as dimers. In contrast, Ni^{2+} induced a change in the oligomerization status of *Vc*Fur. In addition to a peak at 14.5 mL, the chromatogram of Zn_1Ni_1Fur also contained two peaks at 12.7 and 13.5 mL (Fig. 4B), corresponding to species with molecular masses of ~121 and 65 kDa. Therefore, Ni^{2+}-bound Zn_1Fur is a mixture of dimers, tetramers and hexamers, leading to broad bands at 12-15 mL. The small peak at 17.5 mL would be derived from Ni complexes with some components in buffer.

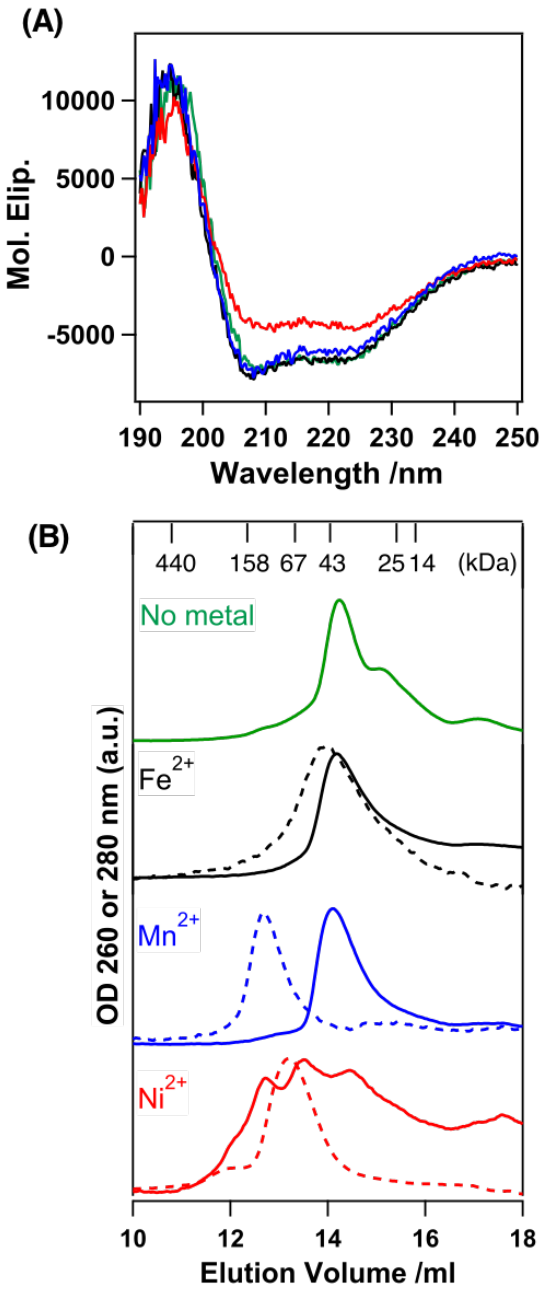

Fig. 4. (A) Far-UV CD spectra of Zn_1Fur (green), Zn_1Fe_1Fur (black), Zn_1Ni_1Fur (red), and Zn_1Mn_1Fur (blue). (B) Elution profile of Zn_1Fur (green), Zn_1Fe_1Fur (black), Zn_1Ni_1Fur (red), and Zn_1Mn_1Fur (blue). Solid and dotted lines indicate absorption of the protein in the absence and presence of the Fur box monitored at 280 and 260 nm, respectively.

We also investigated the oligomerization status of DNA-bound *Vc*Fur using the same size-exclusion chromatography approach. The Zn_1Fe_1Fur-Fur box complex eluted at 13.9 mL, which corresponds to a species with a molecular mass of ~54 kDa (Fig. 4B). Because the combined molecular mass of a single Zn_1Fe_1Fur molecule and the Fur box is 49.6 kDa, a Zn_1Fe_1Fur dimer forms a complex with DNA. In contrast, the Zn_1Ni_1Fur-Fur box complex eluted at 13.2 mL, which corresponds to a species with a molecular mass of ~86 kDa. Moreover, only a single band appeared when Zn_1Ni_1Fur bound to the Fur box. These results show that a Zn_1Ni_1Fur tetramer forms a complex with the Fur box. Finally, the Zn_1Mn_1Fur-Fur box complex eluted at 12.7 mL, corresponding to a species with a molecular mass of ~121 kDa. Therefore, Zn_1Mn_1Fur hexamers form Fur box complex. These results reveal that the association state of *Vc*Fur depends on the metal species. Therefore, the metal species is the factor responsible for determining the structure of *Vc*Fur.

3.4 *Effect of heme binding to VcFur on DNA binding*

Previous studies have shown that Fur proteins from *E. coli* (*Ec*Fur) and *Anabaena* sp. PCC7120 bind to heme [17,18]. Furthermore, in the case of Fur from *Anabaena* sp. PCC7120, DNA binding is inhibited by heme [18]. However, whether *Vc*Fur binds to heme, and if so, whether it would affect DNA binding ability, remains unknown.

To determine whether *Vc*Fur binds heme, we measured UV-Vis absorption spectra of *Vc*Fur after the addition of heme (Fig. S3A). The peak positions of the Soret band of heme in *Vc*Fur solutions were almost the same as those of free heme, suggesting that heme does not bind to *Vc*Fur. However, the possibility that heme is incorporated without coordination to the heme

ligand cannot be ruled out. Therefore, we assessed heme binding based on the intrinsic fluorescence of tyrosine in *Vc*Fur, which contains no tryptophan residues. The fluorescence intensity at 300 nm was reduced upon the addition of heme (Fig. S3B). At a concentration of 2.0 μM, heme reduced the fluorescence intensity at the end of the titration by ~75% compared with that before the addition of heme. Heme decreased the intrinsic fluorescence intensity of *Vc*Fur across its entire concentration range (Fig. 5A), indicating that it binds to Zn_1Fur. The apparent K_d for this interaction, calculated by fitting the fluorescence data to Eq. 3, was 1.1 ± 0.2 μM.

Because a ligand of iron such as histidine can act as a heme ligand, to avoid competition of excess Fe^{2+} with heme, we determined the minimum concentration of Fe^{2+} required for specific binding of Zn_1Fe_1Fur to the Fur box before investigating the effect of heme on *Vc*Fur activity. To this end, we titrated a solution containing Zn_1Fur and 6-FAM–labeled Fur box with Fe^{2+} at 20 °C (Fig. 5B) and found that fluorescence anisotropy reached a plateau at ~10 μM. Thus, subsequent experiments were conducted using 10 μM Fe^{2+} together with 50 nM 6-FAM–labeled Fur box DNA and 6 μM *Vc*Fur.

To investigate whether heme affected the formation of Zn_1Fe_1Fur-Fur box complex, we titrated heme to the complex. Anisotropy decreased with increases in heme concentration, with addition of 10 equivalents of heme (60 μM) to *Vc*Fur inducing almost complete dissociation of *Vc*Fur from the *Vc*Fur-Fur box complex (Fig. 5C). To remove heme from *Vc*Fur, we added 60 μM apomyoglobin to a solution containing 50 nM 6-FAM–labeled Fur box DNA, 6 μM *Vc*Fur, 10 μM Fe^{2+}, and 60 μM heme. This maneuver increased anisotropy from 0.08 to 0.15, indicating that the *Vc*Fur-Fur box complex was restored to its original pre-heme–addition level (Fig. 5C, filled triangle). These results confirm that heme inhibits *Vc*Fur binding to the Fur box.

Because heme inhibits *Vc*Fur activity, we speculated that heme binds in the vicinity of the metal binding sites in *Vc*Fur and competes with metal binding. To test this possibility, we compared the K_d for heme between Zn_1Fur and Zn_1Mn_1Fur. Mn^{2+} was used in these

experiments to mimic the behavior of Fe^{2+}, which is easily oxidized. Heme titration of Zn_1Fur yielded a K_d of 3.8 ± 1.3 μM (Fig. 5D), whereas that for Zn_1Mn_1Fur was 1.4 ± 0.1 μM (Fig. 5E). These results indicate that heme binding to *Vc*Fur is little affected by occupancy of a metal ion at the structural site of *Vc*Fur.

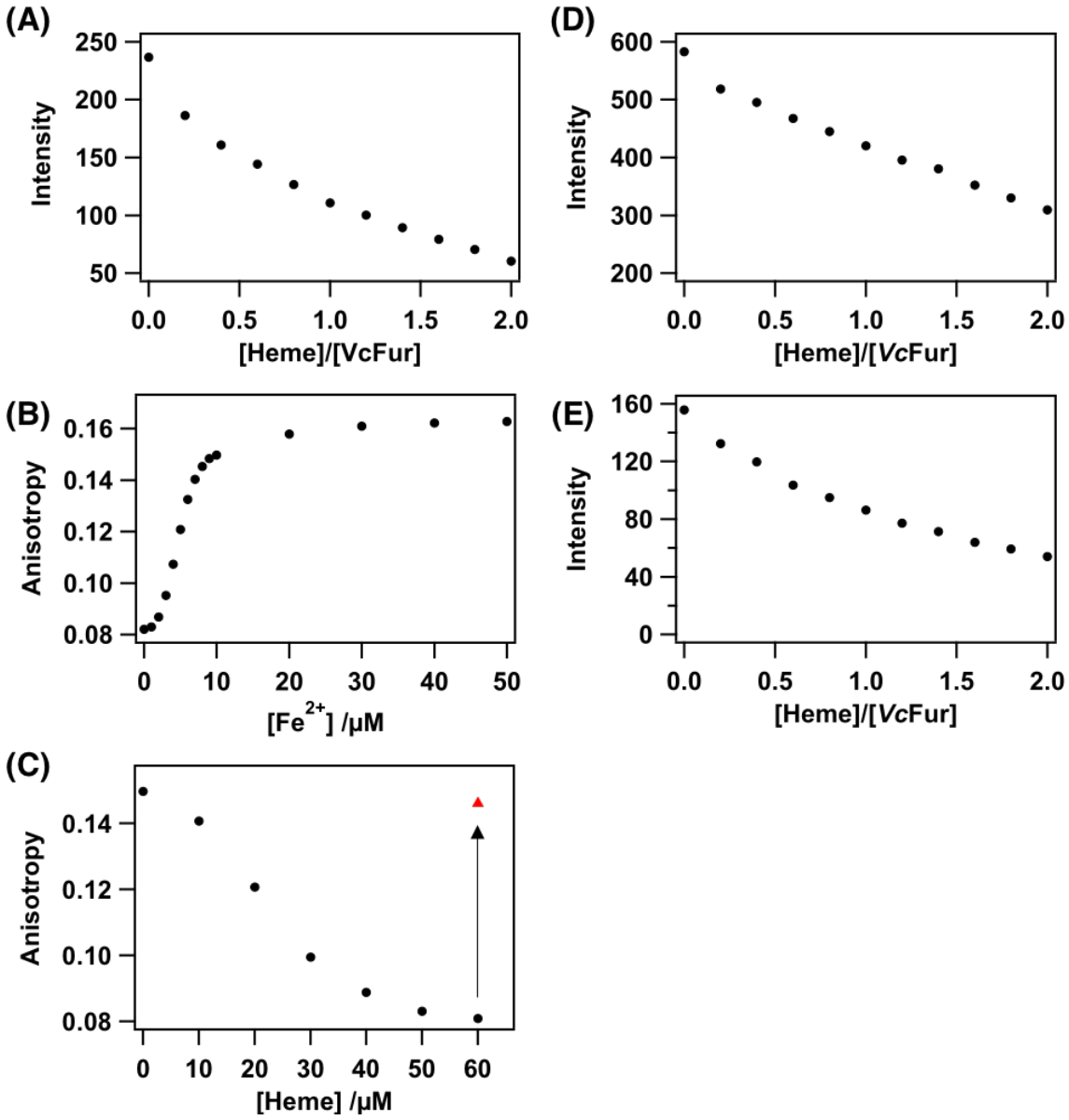

Fig. 5. (A) Heme titration of Zn_1Fur. Control without protein but with tyrosine was subtracted from the respective plots of Zn_1Fur against heme concentration. (B) Fe^{2+} titration of Zn_1Fur. Fluorescence anisotropy of Zn_1Fur (6 μM) in 50 nM 6-FAM–labeled Fur box buffer upon the addition of 0–50 μM Fe^{2+}. (C) Heme titration of *Vc*Fur complexed with Fur box. The plot shows fluorescence anisotropy of 50 nM 6-FAM–labeled Fur box with Zn_1Fur (6 μM) and 10 mM Fe^{2+} as a function of added heme (0–60 μM; black circles). Heme bound to *Vc*Fur was

removed by adding apomyoglobin (60 μM; black triangle) to the *Vc*Fur solution containing 60 μM heme. (D, E) Heme titration of Zn_1Fur (D) and Zn_1Mn_1Fur (E).

3.5 *Heme binding to the nik operon protein, VCA1098*

Our results support the conclusion that expression of the *nik* operon of *V. cholerae* is regulated by Fe^{2+} and heme, but not by Ni^{2+}. We next investigated the possibility that the *nik* operon of *V. cholerae* has functions related to heme and/or iron in addition to the uptake of nickel. In this context, *E. coli* NikA, a *nik* operon-encoded protein (Fig. 1), has been shown to bind to heme [19]. According to a docking simulation of *Ec*NikA and heme using ZDOCK, heme is bound to cleft remote from the nickel-binding cleft [19]. Binding of VCA1098, the *V. cholerae* ortholog of NikA, to heme was assessed by monitoring intrinsic tryptophan fluorescence. In these experiments, in which VCA1098 was excited at 290 nm and fluorescence emission was monitored at 340 nm, the addition of heme resulted in a decrease in fluorescence (Fig. 6A). The apparent K_d, calculated by fitting the fluorescence data to Eq. 3, was 1.31 ± 0.38 μM (Fig. 6B). Upon addition of one equivalent of heme to VCA1098, the peak position of the Soret band remained at 387 nm (Fig. S4)—almost exactly the same position of that of free heme. These results indicate that VCA1098 binds heme but no covalent bond is formed between heme and protein, as is observed with heme binding to NikA.

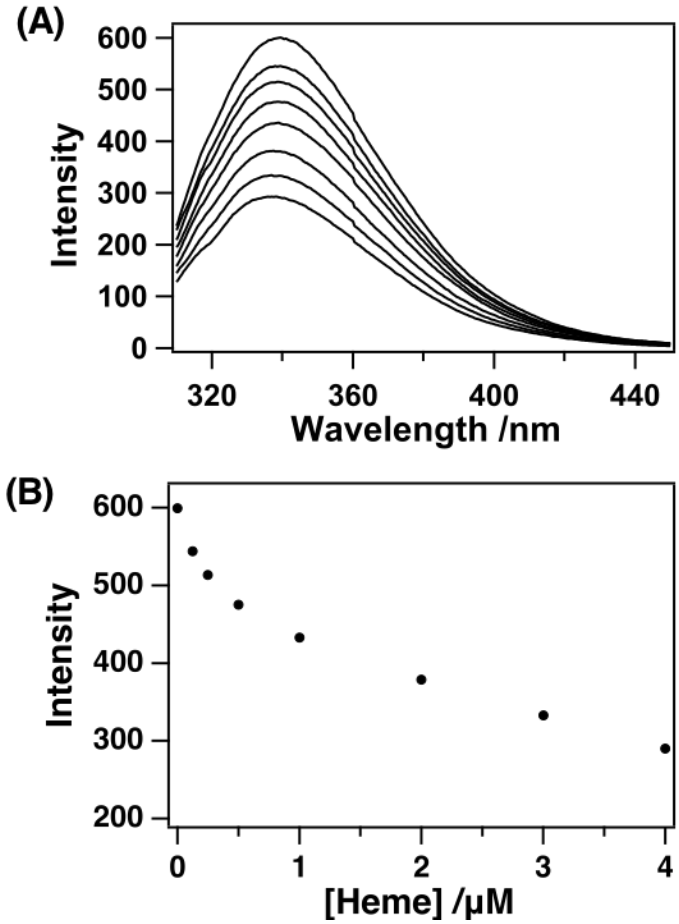

Fig. 6. (A) Heme titration of VCA1098. Fluorescence spectra of VCA1098 in 50 mM Tris-HCl and 150 mM NaCl buffer (pH 8.0) upon the addition of 0–4 equivalents of heme. (B) Plot of fluorescence intensity at 340 nm versus heme concentration.

4. DISCUSSION

4.1 *A metal ion with the proper ionic radius is essential for Fur to specifically recognize the Fur box*

The presence of a Fur box upstream of the *nik* operon of *V. cholerae* (Fig. 1) prompted us to investigate possible Ni^{2+} regulation of the expression of the *nik* operon. Fluorescence anisotropy binding experiments showed that Zn_1Ni_1Fur does not bind specifically to Fur box DNA (Fig. 3A), whereas Zn_1Fe_1Fur does bind specifically with a K_d of 0.99 μM (Fig. 3B). These results suggest that expression of the *nik* operon in *V. cholerae* is regulated by Fe^{2+}, but not Ni^{2+}.

To consider why Zn_1Fe_1Fur, but not Zn_1Ni_1Fur, binds specifically to the Fur box, we investigated structural differences between Zn_1Fe_1Fur and Zn_1Ni_1Fur. Gel-filtration chromatography experiments suggested that Zn_1Fe_1Fur exists as a dimer, whereas Zn_1Ni_1Fur exists as a tetramer (Fig. 4). The reported crystal structure of *Vc*Fur (Zn_2Fur) is a dimeric structure [16]. Although no tetrameric form has been reported for *Vc*Fur, Fur orthologs from *Pseudomonas aeruginosa* (*Pa*Fur) [20] and *Francisella tularensis* (*Ft*Fur) [21] are known to exist as stable tetramers despite their high homology to *Vc*Fur (59% for *Pa*Fur and 42% for *Ft*Fur) [22]. Fur consists of three regions: a DNA binding domain (DBD), a dimerization domain (DD), and a flexible hinge region between DBD and DD (Fig. 7A) [23]. Improper packing of the hinge region between DBD and DD prevents tetramerization. Structural differences between apo- and Fe-bound Fur were detected in the DBDs and hinge region, which exhibited altered conformations. Coordination of Fe^{2+} to Fur at the regulatory site, located in the hinge region, causes a conformational change that leads to stabilization of the hinge conformation, forcing the two DBDs to move closer to each other [23].

Metal ions at the regulatory site of *Vc*Fur are retained by the surrounding three histidine and two glutamic acids (Fig. 7B) [15]. A previous study reported that Fe^{2+} in the regulatory site of *Ec*Fur exists as a high-spin, octahedral species [24,25]. The ionic radius of high-spin Fe^{2+} is 0.78 Å [26], whereas that of Ni^{2+} is 0.55–0.69 Å, depending on the coordination number (4–6) [26]. Thus, the ionic radius of Ni^{2+} is smaller than that of Fe^{2+} by 0.1–0.2 Å. Ni^{2+} binding might cause the DBD to be pulled toward DD to a larger extent than Fe^{2+} binding. Therefore, this difference in conformational change between DBD and DD would lead to a change in the oligomerization status between Zn_1Ni_1Fur and Zn_1Fe_1Fur.

In contrast to Ni^{2+}- and Fe^{2+}-bound Fur, Mn^{2+}-bound *Vc*Fur adopts a hexametric form (Fig. 4B). Mn^{2+}, like Fe^{2+}, exists as an octahedral structure in *Ec*Fur [27]. The ionic radius of Mn^{2+} is 0.83 Å, which is 0.05 and >0.14 Å larger than that of Fe^{2+} and Ni^{2+}, respectively [26]. Therefore, coordination of Mn^{2+} with *Vc*Fur may weaken the attraction of the two DBDs in a

dimer. As a result, Zn_1Mn_1Fur would more easily form a hexamer. Accordingly, the DNA-binding ability of *Vc*Fur may be regulated by changes in the alignment of the DBD through coordination of metal ions to the regulatory site.

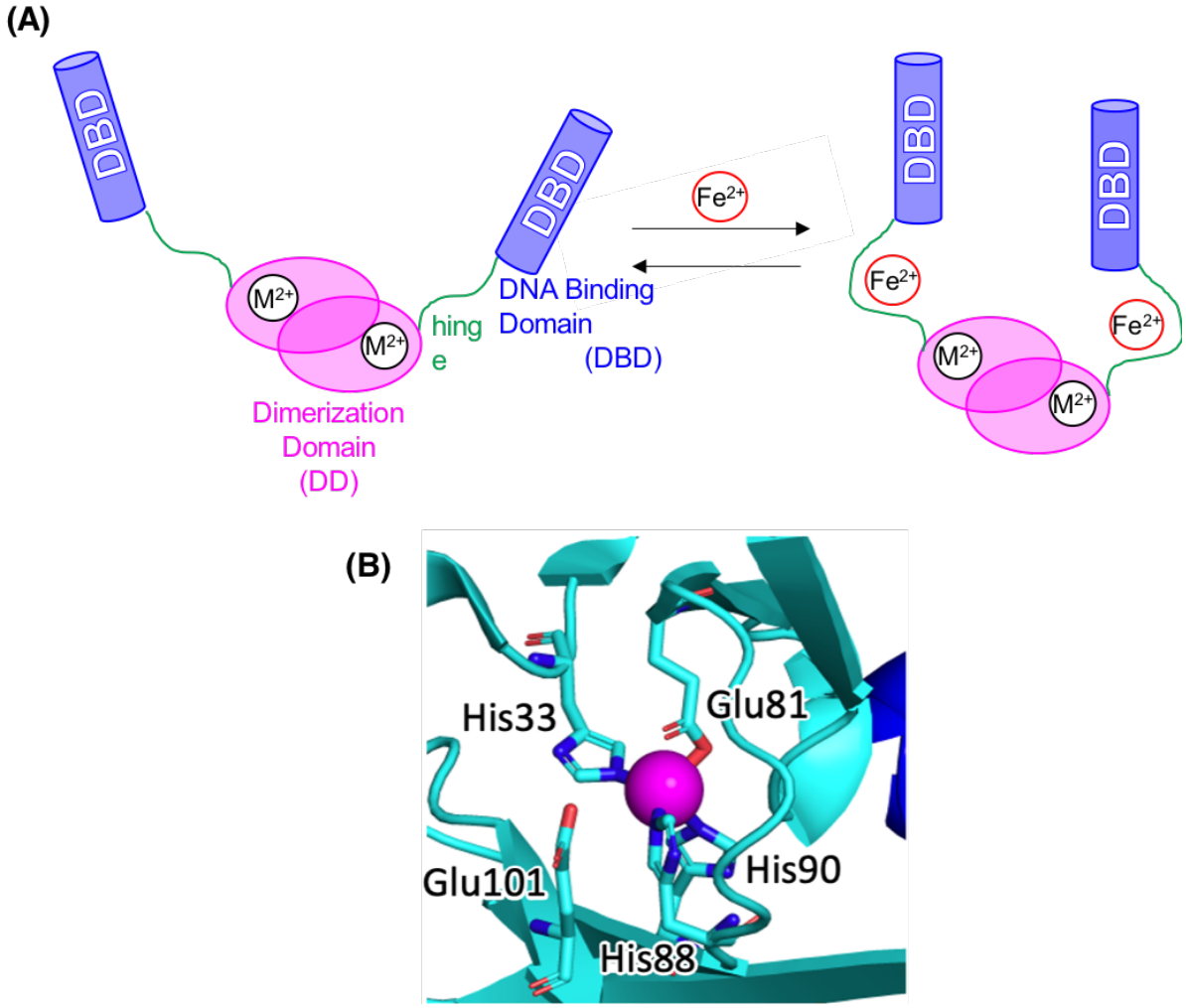

Fig. 7. (A) Model of the metal-induced conformational change in *Vc*Fur. Of the two metal binding sites of *Vc*Fur, the site in the hinge region is the regulatory site. Binding of metal to this site induces a structural change in the hinge that leads to closer packing of the DBD, which facilitates binding to DNA. (B) X-ray crystal structure of the local structural site of *Vc*Fur (PDBID: 2W57).

4.2 *Heme inhibits Fur binding to the Fur box*

As described above, Fe^{2+}, but not Ni^{2+}, regulates the expression of the *nik* operon of *V. cholerae*. Regulation of the function of Irr, an iron-responsive regulator and heme-binding

member of the Fur superfamily [28], depends on heme as well as iron [29]. *Vc*Fur also binds heme with a K_d of 1.1 μM (Fig. 5A). As is the case for Irr [29], heme binding almost completely inhibited *Vc*Fur from binding to the Fur box (Fig. 5C). Irr regulates the expression of *hem*B, encoding the heme biosynthetic enzyme ALA dehydratase, and thereby contributes to increase in the amount of heme in cells. Under conditions of heme excess, heme binds to Irr and derepresses the expression of *hemB*, promoting heme synthesis [30].

Expression of the *nik* operon of *V. cholerae* is suppressed when iron is in excess [11] and increased when heme is in excess. Since the *nik* operon in *V. cholerae* encodes an ABC transporter that transports nickel from the periplasm to the cytosol (Fig. 1), it is possible that *V. cholerae* regulates nickel uptake by iron and heme. Fur regulates many genes essential for *V. cholerae* growth, such as siderophore synthesis and transport, the TonB system, and iron storage [31]. In particular, the Hut system, important for the uptake and degradation of heme from the exterior environment of *V. cholerae*, is also regulated by *Vc*Fur [31,32]. Therefore, in the presence of excess heme in *V. cholerae*, binding of heme to *Vc*Fur causes dissociation of *Vc*Fur from the Fur box and increases the expression of Hut proteins, which may accelerate heme uptake and degradation. Therefore, the fact that Fur is an important regulator of iron metabolism in *V. cholerae* [11,31] taken together with the presence of a Fur box upstream of the *nik* operon suggest that the *nik* operon is involved in iron and heme metabolism and may play an important role in the growth of *V. cholerae*. Conceivably, nickel is involved in a cofactor of [NiFe]-hydrogenase, which contributes to the production of H_2 in anaerobic metabolism [33,34], in Gram-negative bacteria such as *E. coli*. [NiFe]-hydrogenase is also present in *V. cholerae*. Ferrous irons in cells under an anaerobic condition are used for cofactors of iron-containing proteins such as [NiFe]-hydrogenase, leading to starvation of iron. Because Fur induces expression of *nik* operon at lower concentration of iron [11], this is a possible scenario of regulation of *nik* operon expression according to the intracellular iron concentration.

4.3. *Possible involvement of VCA1098 in heme metabolism*

VCA1098 is a protein encoded by the *nik* operon (Fig. 1). Thus, the expression of VCA1098 is regulated by Fe^{2+} and heme via *Vc*Fur. A VCA1098 deficiency has been shown to reduce the susceptibility of *V. cholerae* to extracellular nickel [11]. Moreover, VCA1098 shares high homology with *E. coli* NikA, a nickel-binding periplasmic protein that is part of a nickel ABC transport system [35]. These results suggest that VCA1098 may be a nickel transporter.

VCA1098 binds to heme with a K_d of 1.1 μM (Fig. 6). However, no covalent bond is formed between heme and VCA1098. NikA does not bind metal ions as a bare ion, but binds via a chelated molecule like a siderophore [8]. NikA may be involved in iron uptake by binding to heme as well as siderophore and taking up heme in a manner similar to nickel. Thus, VCA1098 may have two roles: nickel uptake and iron/heme utilization. Regulation of the expression of VCA1098 by iron, heme and Fur also supports the involvement of VCA1098 in heme metabolism.

5. Conclusions

In summary, starting from the observation that a Fur box is present upstream of the *nik* operon, which encodes the nickel-uptake system of *V. cholerae*, we investigated regulation of the expression of the *nik* operon, discovering that it is regulated by Fur in a manner that depends on the intracellular concentration of iron and heme, but not nickel. Furthermore, we revealed that heme binds to VCA1098, which is encoded by the *nik* operon. These results suggest that the *nik* operon is involved not only in nickel uptake but also in iron and heme metabolism. A more detailed investigation of these regulatory features can be expected to elucidate new aspects of *V. cholerae* growth mechanisms.

Acknowledgements

We would like to express our gratitude to Ms. N. Takeda, Open Facility Division, Global

Facility Center, Creative Research Institution, Hokkaido University for elemental analysis using ICP-AES and providing insight and expertise that greatly assisted the research. We also thank Mr. Kentaro Doi for his help with expression of *Vc*Fur.

Funding

This work was supported by JSPS KAKENHI Grant Numbers JP19H05769 (K.I.), JP20K05700 (T.U), and JP21J11192 (K.M.).

REFERENCES

[1] H. De Reuse, D. Vinella, C. Cavazza, Common themes and unique proteins for the uptake and trafficking of nickel, a metal essential for the virulence of *Helicobacter pylori*, *Front. Cell. Infect. Microbiol.* 3 (2013) 1–6. https://doi.org/10.3389/fcimb.2013.00094.

[2] J.W. Olson, N.S. Mehta, R.J. Maier, Requirement of nickel metabolism proteins HypA and HypB for full activity of both hydrogenase and urease in *Helicobacter pylori*, *Mol. Microbiol.* 39 (2001) 176–182. https://doi.org/10.1046/j.1365-2958.2001.02244.x.

[3] K.A. Eaton, S. Krakowka, Effect of gastric pH on urease-dependent colonization of gnotobiotic piglets by *Helicobacter pylori*, *Infect. Immun.* 62 (1994) 3604–3607. https://doi.org/10.1128/iai.62.9.3604-3607.1994.

[4] K.A. Andrutis, J.G. Fox, D.B. Schauer, R.P. Marini, J.C. Murphy, L. Yan, J. V. Solnick, Inability of an isogenic urease-negative mutant strain of *Helicobacter mustelae* to colonize the ferret stomach, *Infect. Immun.* 63 (1995) 3722–3725. https://doi.org/10.1128/iai.63.9.3722-3725.1995.

[5] M. Tsuda, M. Karita, M.G. Morshed, K. Okita, T. Nakazawa, A urease-negative mutant of *Helicobacter pylori* constructed by allelic exchange mutagenesis lacks the ability to colonize the nude mouse stomach, *Infect. Immun.* 62 (1994) 3586–3589. https://doi.org/10.1128/iai.62.8.3586-3589.1994.

[6] K. Schauer, B. Gouget, M. Carrière, A. Labigne, H. De Reuse, Novel nickel transport mechanism across the bacterial outer membrane energized by the TonB/ExbB/ExbD machinery, *Mol. Microbiol.* 63 (2007) 1054–1068. https://doi.org/10.1111/j.1365-2958.2006.05578.x.

[7] C. Navarro, L. -F Wu, M. -A Mandrand-Berthelot, The nik operon of *Escherichia coli* encodes a periplasmic binding-protein-dependent transport system for nickel, *Mol.*

Microbiol. 9 (1993) 1181–1191. https://doi.org/10.1111/j.1365-2958.1993.tb01247.x.

[8] M. V. Cherrier, C. Cavazza, C. Bochot, D. Lemaire, J.C. Fontecilla-Camps, Structural characterization of a putative endogenous metal chelator in the periplasmic nickel transporter NikA, *Biochemistry.* 47 (2008) 9937–9943. https://doi.org/10.1021/bi801051y.

[9] K. De Pina, V. Desjardin, M.A. Mandrand-Berthelot, G. Giordano, L.F. Wu, Isolation and characterization of the nikR gene encoding a nickel- responsive regulator in *Escherichia coli*, *J. Bacteriol.* 181 (1999) 670–674. https://doi.org/10.1128/jb.181.2.670-674.1999.

[10] Y. Kang, K.D. Weber, Y. Qiu, P.J. Kiley, F.R. Blattner, Genome-wide expression analysis indicates that FNR of *Escherichia coli* K-12 regulates a large number of genes of unknown function, *J. Bacteriol.* 187 (2005) 1135–1160. https://doi.org/10.1128/JB.187.3.1135-1160.2005.

[11] B.W. Davies, R.W. Bogard, J.J. Mekalanos, Mapping the regulon of *Vibrio cholerae* ferric uptake regulator expands its known network of gene regulation, *Proc. Natl. Acad. Sci. U. S. A.* 108 (2011) 12467–12472. https://doi.org/10.1073/pnas.1107894108.

[12] E. Pohl, J.C. Haller, A. Mijovilovich, W. Meyer-Klaucke, E. Garman, M.L. Vasil, Architecture of a protein central to iron homeostasis: Crystal structure and spectroscopic analysis of the ferric uptake regulator, *Mol. Microbiol.* 47 (2003) 903–915. https://doi.org/10.1046/j.1365-2958.2003.03337.x.

[13] S.A. Mills, M.A. Marletta, Metal Binding Characteristics and Role of Iron Oxidation in the Ferric Uptake Regulator from *Escherichia coli* , *Biochemistry.* (2005) 13553–13559. https://doi.org/10.1021/bi0507579.

[14] T. Uchida, M. Sasaki, Y. Tanaka, K. Ishimori, A Dye-Decolorizing Peroxidase from *Vibrio cholerae*, *Biochemistry.* 54 (2015) 6610–6621.

https://doi.org/10.1021/acs.biochem.5b00952.

[15] M.A. Sheikh, G.L. Taylor, Crystal structure of the *Vibrio cholerae* ferric uptake regulator (Fur) reveals insights into metal co-ordination, *Mol. Microbiol.* 72 (2009) 1208–1220. https://doi.org/10.1111/j.1365-2958.2009.06718.x.

[16] J.J. Gilbreath, O.Q. Pich, S.L. Benoit, A.N. Besold, J.H. Cha, R.J. Maier, S.L.J. Michel, E.L. Maynard, D.S. Merrell, Random and site-specific mutagenesis of the *Helicobacter pylori* ferric uptake regulator provides insight into Fur structure-function relationships, *Mol. Microbiol.* 89 (2013) 304–323. https://doi.org/10.1111/mmi.12278.

[17] A. Smith, N.I. Hooper, N. Shipulina, W.T. Morgan, Heme binding by a bacterial repressor protein, the gene product of the ferric uptake regulation (fur) gene of *Escherichia coli*, *J. Protein Chem.* 15 (1996) 575–583. https://doi.org/10.1007/BF01908539.

[18] J.A. Hernández, M.L. Peleato, M.F. Fillat, M.T. Bes, Heme binds to and inhibits the DNA-binding activity of the global regulator FurA from *Anabaena* sp. PCC 7120, *FEBS Lett.* 577 (2004) 35–41. https://doi.org/10.1016/j.febslet.2004.09.060.

[19] M. Shepherd, M.D. Heath, R.K. Poole, NikA binds heme: A new role for an *Escherichia coli* periplasmic nickel-binding protein, *Biochemistry.* 46 (2007) 5030–5037. https://doi.org/10.1021/bi700183u.

[20] J. Pérard, J. Covès, M. Castellan, C. Solard, M. Savard, R. Miras, S. Galop, L. Signor, S. Crouzy, I. Michaud-Soret, E. De Rosny, Quaternary Structure of fur Proteins, a New Subfamily of Tetrameric Proteins, *Biochemistry.* 55 (2016) 1503–1515. https://doi.org/10.1021/acs.biochem.5b01061.

[21] J. Pérard, S. Nader, M. Levert, L. Arnaud, P. Carpentier, C. Siebert, F. Blanquet, C. Cavazza, P. Renesto, D. Schneider, M. Maurin, J. Coves, S. Crouzy, I. Michaud-Soret, Structural and functional studies of the metalloregulator Fur identify a promoter-binding mechanism and its role in *Francisella tularensis virulence*, *Commun. Biol.* 1

(2018). https://doi.org/10.1038/s42003-018-0095-6.

[22] S. Nader, J. Pérard, P. Carpentier, L. Arnaud, S. Crouzy, I. Michaud-Soret, New insights into the tetrameric family of the Fur metalloregulators, *BioMetals.* 32 (2019) 501–519. https://doi.org/10.1007/s10534-019-00201-8.

[23] Z. Deng, Q. Wang, Z. Liu, M. Zhang, A.C.D. Machado, T.P. Chiu, C. Feng, Q. Zhang, L. Yu, L. Qi, J. Zheng, X. Wang, X.M. Huo, X. Qi, X. Li, W. Wu, R. Rohs, Y. Li, Z. Chen, Mechanistic insights into metal ion activation and operator recognition by the ferric uptake regulator, *Nat. Commun.* 6 (2015). https://doi.org/10.1038/ncomms8642.

[24] M.Y. Hamed, J.B. Neilands, V. Huynh, Binding of the ferric uptake regulation repressor protein (Fur) to Mn(II), Fe(II), Co(II), and Cu(II) ions as co-repressors: Electronic absorption, equilibrium, and 57Fe Mössbauer studies, *J. Inorg. Biochem.* 50 (1993) 193–210. https://doi.org/10.1016/0162-0134(93)80025-5.

[25] J. Katigbak, Y. Zhang, Iron binding site in a global regulator in bacteria-ferric uptake regulator (fur) protein: Structure, Mössbauer properties, and functional implication, *J. Phys. Chem. Lett.* 3 (2012) 3503–3508. https://doi.org/10.1021/jz301689b.

[26] R. D. SHANNON, Revised effective ionic radii and systematic studies of interatomic distances in halides and chalcogenides, *Acta Crystallogr. Sect. A.* A32 (1976) 751–767. https://doi.org/10.1107/S0567739476001551.

[27] M.Y. Hamed, J.B. Neilands, An electron spin resonance study of the Mn(II) and Cu(II) complexes of the Fur repressor protein, *J. Inorg. Biochem.* 53 (1994) 235–248. https://doi.org/10.1016/0162-0134(94)85111-5.

[28] Z. Qi, I. Hamza, M.R. O'Brian, Heme is an effector molecule for iron-dependent degradation of the bacterial iron response regulator (Irr) protein, *Proc. Natl. Acad. Sci. U. S. A.* 96 (1999) 13056–13061. https://doi.org/10.1073/pnas.96.23.13056.

[29] D. Nam, Y. Matsumoto, T. Uchida, M.R. O'Brian, K. Ishimori, Mechanistic insights into heme-mediated transcriptional regulation via a bacterial manganese-binding iron

regulator, iron response regulator (Irr), *J. Biol. Chem.* 295 (2020) 11316–11325. https://doi.org/10.1074/jbc.ra119.011855.

[30] I. Hamza, S. Chauhan, R. Hassett, M.R. O'Brian, The bacterial irr protein is required for coordination of heme biosynthesis with iron availability, *J. Biol. Chem.* 273 (1998) 21669–21674. https://doi.org/10.1074/jbc.273.34.21669.

[31] A.R. Mey, E.E. Wyckoff, V. Kanukurthy, C.R. Fisher, S.M. Payne, Iron and Fur Regulation in *Vibrio cholerae* and the Role of Fur in Virulence, *Infect. Immun.* 73 (2005) 8167–8178. https://doi.org/10.1128/IAI.73.12.8167.

[32] T. Uchida, Y. Sekine, T. Matsui, M. Ikeda-Saito, K. Ishimori, A heme degradation enzyme, HutZ, from *Vibrio cholerae*, *Chem. Commun.* 48 (2012) 6741–6743. https://doi.org/10.1039/c2cc31147j.

[33] M.C. Schoelmerich, V. Müller, Energy-converting hydrogenases: the link between H_2 metabolism and energy conservation, *Cell. Mol. Life Sci.* 77 (2020) 1461–1481. https://doi.org/10.1007/s00018-019-03329-5.

[34] P.M. Vignais, B. Billoud, J. Meyer, Classification and phylogeny of hydrogenases, *FEMS Microbiol.* Rev. 25 (2001) 455–501. https://doi.org/10.1016/S0168-6445(01)00063-8.

[35] C. Navarro, L.-F. Wu, M.-A. Mandrand-Berthelot, The nik operon of *Escherichia coli* encodes a periplasmic binding-protein-dependent transport system for nickel, *Mol. Microbiol.* 9 (1993) 1181–1191. https://doi.org/10.1111/j.1365-2958.1993.tb01247.x.

FIGURE LEGENDS

Fig. 1. Comparison of the *nik* operon between *E. coli* K-12 and *V. cholerae* O1 El Tor. Genes and arrows indicating the extent of the *nik* operons are color-coded to facilitate comparison. Proteins localized in the periplasm are displayed in orange, transmembrane proteins are displayed in green, and proteins localized in the cytoplasm are displayed in magenta. The *nikR* gene, located downstream of the FNR box in *E. coli* but absent in *V. cholerae*, is colored purple. A Fur box (white box) is located upstream of the *nik* operon of *V. cholerae*, whereas a FNR box (red box) is located upstream of the *nik* operon of *E. coli*. Filled arrows are drawn to scale and accurately positioned based on the genome sequences depicted.

Fig. 2. (A) Representative Coomassie Brilliant Blue-stained SDS-PAGE gel showing purified *Vc*Fur. (B) Elution profile of purified *Vc*Fur on a Bio-Rad Enrich SEC 650 column monitored at 280 nm.

Fig. 3. Binding of *Vc*Fur to the Fur box. Fluorescence anisotropy data of (A) Zn_1Ni_1Fur, (B) Zn_1Fe_1Fur, and (C) Zn_1Mn_1Fur. Titration was performed using 50 nM 6-FAM–labeled Fur box. In each graph, the anisotropy of Zn_1Fur is shown by open circles. The anisotropy of metal-bound *Vc*Fur (Zn_1M_1Fur) in the absence and presence of 200 μg mL^{-1} of ssDNA is shown as filled circles and triangles, respectively.

Fig. 4. (A) Far-UV CD spectra of Zn_1Fur (green), Zn_1Fe_1Fur (black), Zn_1Ni_1Fur (red), and Zn_1Mn_1Fur (blue). (B) Elution profile of Zn_1Fur (green), Zn_1Fe_1Fur (black), Zn_1Ni_1Fur (red), and Zn_1Mn_1Fur (blue). Solid and dotted lines indicate fluorescence of the protein in the absence and presence of the Fur box, respectively, monitored at 280 and 260 nm.

Fig. 5. (A) Heme titration of Zn_1Fur. Control without protein but with tyrosine was subtracted

from the respective plots of Zn_1Fur against heme concentration. (B) Fe^{2+} titration of Zn_1Fur. Fluorescence anisotropy of Zn_1Fur (6 μM) in 50 nM 6-FAM–labeled Fur box buffer upon the addition of 0–50 μM Fe^{2+}. (C) Heme titration of *Vc*Fur complexed with Fur box. The plot shows fluorescence anisotropy of 50 nM 6-FAM–labeled Fur box with Zn_1Fur (6 μM) and 10 μM Fe^{2+} as a function of added heme (0–60 μM; black circles). Heme bound to *Vc*Fur was removed by adding apomyoglobin (60 μM; black triangle) to the *Vc*Fur solution containing 60 μM heme. (D, E) Heme titration of Zn_1Fur (D) and Zn_1Mn_1Fur (E).

Fig. 6. (A) Heme titration of VCA1098. Fluorescence spectra of VCA1098 in 50 mM Tris-HCl and 150 mM NaCl buffer (pH 8.0) upon the addition of 0–4 equivalents of heme. (B) Plot of fluorescence intensity at 340 nm versus heme concentration.

Fig. 7. (A) Model of the metal-induced conformational change in *Vc*Fur. Of the two metal binding sites of *Vc*Fur, the site in the hinge region is the regulatory site. Binding of metal to this site induces a structural change in the hinge that leads to closer packing of the DBD, which facilitates binding to DNA. (B) X-ray crystal structure of the local structural site of *Vc*Fur (PDBID: 2W57).